Alignment and statistical analysis of 2D small-scale paper property maps

MARJA R. METTÄNEN[1], HEIMO A.T. IHALAINEN[2] AND RISTO K. RITALA[3]

SUMMARY

The relationship between printability and paper structure based on registration, alignment and analysis of 2D property maps of unprinted and printed paper has been studied. Surface topography, optical formation and intensity of the print were all measured and the point-by-point probabilistic interdependencies of these properties statistically characterised. The 2D measurements of the paper properties and the print quality were aligned with a point-mapping based registration procedure. This alignment provides a large amount of multivariate pointwise data and thus permits reliable estimates of the joint probability density functions (pdfs) that are efficiently parameterized through Gaussian mixtures. Assuming the interdependency to be only probabilistic and non-Gaussian, it is possible to derive full conditional pdfs instead of regression models and to investigate how the shape of the conditional pdfs – e.g. tails – depends on the conditioning variable. These pdfs were used to form anomaly maps that locate defects (for example, print defects) and their causes. The methods and the usefulness of the analyses were demonstrated with results on newsprint samples.

KEYWORDS

Image registration, multivariate statistical analysis, paper properties, printability, joint probability distributions

INTRODUCTION

Small-scale 2D measurements of paper produce considerable amount of useful information about the physical parameters of the fibre network and paper surface properties (*1-3*). The measurements are

[1]Research Scientist, PhD Student and corresponding author (marja.mettanen@tut.fi), [2]Laboratory Engineer, [3]Professor
  Department of Automation Science and Engineering
  Tampere University of Technology
  P.O. Box 692, FI-33101 Tampere, Finland

made with various devices and sensor matrices and thus the sets of property maps obtained typically have neither the same size nor the same resolution. To take full advantage of the 2D measurements acquired from the same area of a paper sheet, methods for image registration and alignment are required in order to overlay the measured images so that the pixels with the same physical coordinates in the different images, corresponding to the same part of the sample, can be compared. This is a pre-requisite for reliable joint analysis of the maps. The idea of aligned image analysis has been used in paper physics recently by, e.g. Sung et al. (*4*) who computed maps of apparent density of paper from aligned 2D measurements of thickness and formation. A wide range of material characterization and analysis applications could possibly benefit from aligned multi-channel maps that typically contain a large number of independently measured data points, as this would set up a firm basis for statistical analysis of the measured properties. Analyzing the microstructure of paper through the aligned measurement maps is further motivated by the fact that the physical characteristics of paper are associated with printability and with the quality of the final printed product (*5-7*). Previous studies utilizing aligned images have shown this using correlation and regression analysis (*8-10*). There is no questioning of the significance of these results, but it can be expected that traditional statistical analysis methods, such as regression analysis, do not provide full information about the dependencies between measured print quality and the structural parameters because the dependencies are statistical and non-Gaussian. Regression provides the expected value of the target variable given the values of the explanatory variables but neglects prediction uncertainty that tends to be large due to the effects of the printing process and unmeasured properties of paper. The key idea in the current work is to approach the dependencies through the full joint probability densities of the measured properties, as these provide not only regression

but full parametric descriptions of the statistical relationships. The long-term goal in this research is to gain understanding and to generate models of the relationships between the statistical properties of print quality and the measurable physical structure of unprinted paper so that paper quality can be effectively monitored.

The intense development of image acquisition and analysis techniques has led to a wide variety of registration and alignment tools in application areas such as remote sensing, image fusion, stereo vision, super-resolution, close-range photogrammetry, and medical imaging (*11*). Various image registration methods have been reported to assist in automatic image registration, e.g. (*12,13*), however none of the methods published so far have been readily applicable to the automatic registration of randomly textured image data sets (such as the 2D small-scale maps of paper structure) that contain no special registration marks. The authors have previously developed a new method for that purpose and verified its usability by several registration experiments with multimodal 2D measurement data (*14*).

A methodology for the multivariate statistical analysis of aligned 2D property maps of paper measured before and after printing is proposed. A block diagram of the analysis procedure is presented in Figure 1. After aligning the measured small-scale maps accurately it is possible to compare the measured properties point-by-point and gain fundamental information about the physical mechanisms determining the quality of paper and print. It can be expected that, however accurate the measurements, there are no deterministic point-to-point relationships between print quality and the structural properties. Instead, the relationships are probabilistic and thus they are appropriately described with the full joint probability distributions of the measured properties (*15*). The joint distributions are typically clearly different from multivariate Gaussian and thus cannot be summarized with one expectation vector and covariance matrix. On the other hand, distribution models that assume the third, fourth or higher
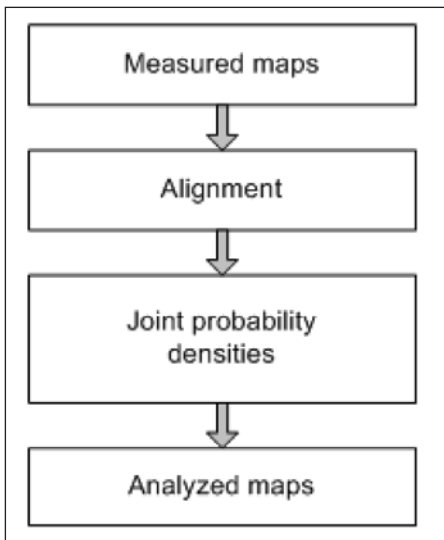
Fig. 1 Multivariate analysis procedure.

moments fixed would be only numerically solvable. An alternative description of the distributions with histograms or Gaussian mixture models (GMM) (*16*) can be adopted. The GMM approach is particularly attractive for two main reasons. Firstly, GMM can condense the huge amount of data into a fairly small set of parameters. Secondly, this parametric representation generally enables the analytical calculation of conditional probability density functions (pdfs) of individual quality properties. It should be noted however, that in some cases the very fine details in the tails of the pdfs can be effectively analyzed only with histograms, as is shown later. The large number of independently measured data points in the multivariate images provides a strong basis for pdf estimation and statistical inference. It is possible to examine the shape of the distributions and use the joint pdf models to derive anomaly maps of the measured properties. Anomaly maps reveal the points and areas that deviate most strongly from the typical statistical behavior, thus providing essential information of, for example, print defects and their origins.

The authors have previously examined the correspondence of different paper surface topography measurement devices (*14*) through multivariate image analysis. The research described here goes further in the analysis of paper structure and reports experiments with 2D measurements of surface topography, optical formation and print quality. Similar research has been conducted before but with only 1 mm resolution (*17*). The resolution in the property maps analysed here is 0.01 mm. The example cases present the analysis of

newsprint samples that have been printed with a sheet-fed offset press.

The body of the paper is organized as follows. First a description of the new automatic image registration method is given and its requirements and accuracy discussed. The property maps measured from the samples both before and after printing are then introduced. The multivariate statistical analysis method employing joint probability densities and the application of the tools to the aligned maps is then described. Finally, results from the analysis are presented and the information provided by these analytical methods discussed.

ALIGNMENT OF MEASURED MAPS

The registration and alignment of two images, one a reference and the other referred to as input, describes the process whereby the input image is spatially transformed to overlay it with the reference image. The image registration procedure consists of two phases. They are both based on point mapping which is the primary approach used to register images with random textures (*11*). The similarity of the images is measured by normalized cross-correlation (*15*). Furthermore, it is assumed that a global affine transformation (*18*) is sufficient to bring the corresponding coordinates of the reference and input images together. This assumption is simply based on earlier experience with misregistration between the measured property maps. The major causes of misregistration in the 2D measurements are known to be due to different resolution of the measurements and minor error in orientation between the sample and the measuring device. It is also possible that there is a slight obliqueness, for example due to optical imperfections. Affine transformation can model and correct all these effects with six parameters.

The registration is in two phases for accuracy, computational efficiency, and robustness. A coarse approximation for plain translation is first identified and then refined iteratively. The first phase begins by placing a set of nine control points close to the center of the reference map, as illustrated in Figure 2. Small areas around the control points are selected and similar areas are searched from the input image to locate the matching points. At each control point, the estimate of the translation between the images is determined by the position of the maximum of the 2D cross-correlation function. Since

not all the control points require exactly the same translation between the reference and input images, the weighted median value of the nine translation estimates, in both horizontal and vertical directions is chosen as the first phase estimate. Choosing median rather than mean is for robustness.

The second registration phase generalizes the transformation estimate from plain translation to affine transformation. It is an iterative process that gradually refines the transformation estimate. At each iteration step, a set of new control points is automatically positioned on the reference image, and the locations of these points in the input image are predicted with the transformation estimate from the previous iteration step. The exact locations of the matching points are again chosen at the maxima of the 2D cross-correlation function. Since an estimate of the required transformation exists, the search area size in the similarity maximization is considerably smaller than in the first stage. This makes the point search computationally efficient. The locations of the matching points are determined at sub-pixel accuracy by fitting a second order 2D polynomial around the maximum of the cross-correlation function. At the end of each iteration step, the matching control points found so far are used to form a new transformation estimate. A global affine transformation is fitted between the matching control points using a weighted least squares approach so that the effect of abnormal control point pairs is minimized.

The control points selected during the iteration gradually cover the image all the way to the corners of the reference image, thus improving the overall registration accuracy. When the grid of control points finally covers the joint area of the reference and input images, the iterative procedure is terminated and the final affine transformation is fitted between the matching control points. This automatic registration procedure has been tested with many 2D quality maps of both paper and board and affine transformations were found to be appropriate in all cases and the alignment method was accurate and robust. The transformation fitting error is normally less than 0.3 pixels. Obviously, when the two maps to be aligned do not have common forms of variation, the method fails.

The final part of the registration is image alignment in which the estimated transformation is applied to the coordinates of the input image. Pixel values are then interpolated to the new non-integer
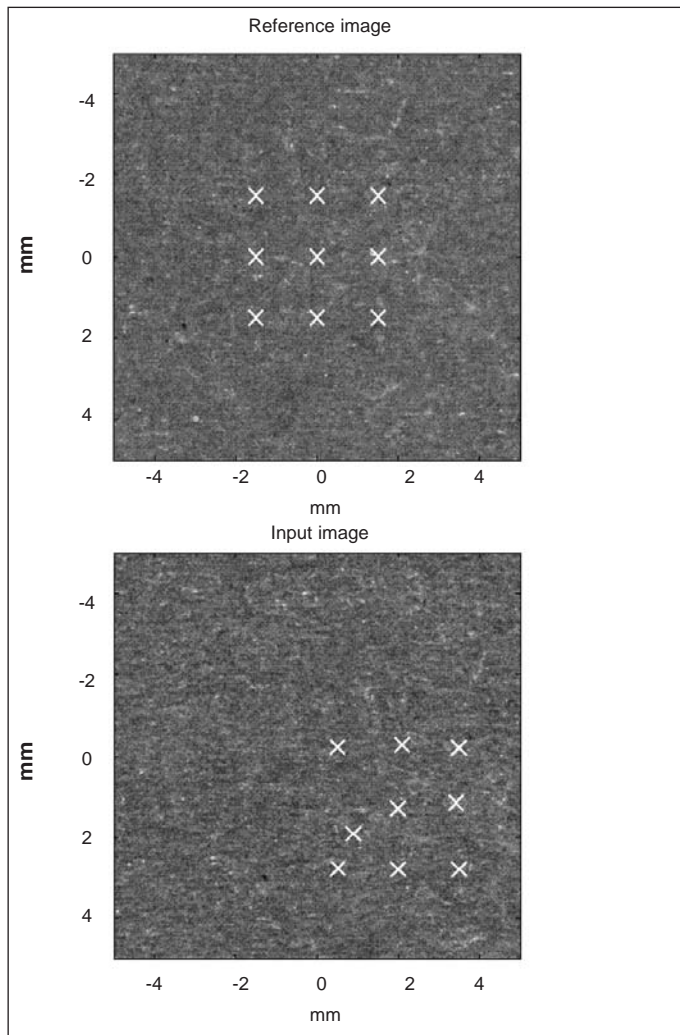
Fig. 2 Estimation of translation at the first phase of image registration. Reference image with search points (top) and input image with found points (bottom). The true translation is [2.0 1.3] mm ([x y]).

scanning. Understanding and combining the information on the colour channels is essential in the multivariate analysis of the aligned maps, but also in image registration because the reference and input images should contain maximally common forms of variation to provide accurate registration results.

The image registration procedure described previously has proven to be capable of successfully registering this diverse set of 2D measurements acquired from halftone and compact colour areas. The registration results even revealed the slight geometric distortions in the camera images caused by the optics. It is possible to implement camera calibration to maximize the usable measurement area, but for the current measurements, only the parts of the images with less than a half pixel dislocation were selected for the analysis. Even though this reduced the analyzed area from the original size of 22 by 15 mm, extensive amounts of multivariate image data were obtained; on each test area the number of observations was always more than two million. So far statistical analysis has been restricted to the 2D measurements collected from two different types of compact cyan areas that will be described later in more detail.

In addition to camera calibration, these registration and alignment methods rapidly revealed a subtle twitching of the read head of the scanner that was not discernible by naked eye during the measurement. They also revealed that the target often was slightly out of focus in the scanner measurements. Due to these imperfections, optical formation measurements were not analyzed further. To replace the suboptimal scanner measurement in the future, a camera-based device for the measurement of optical formation has already been constructed, that is expected to give sharper images and better dynamics in particular with the unprinted paper that has been problematic for the scanner.

MULTIVARIATE STATISTICAL ANALYSIS THROUGH JOINT PROBABILITY DISTRIBUTIONS

In what follows, random variables are denoted with upper case letters and the values they take with corresponding lower case letters.

The general form of the joint probability density function of random variables (vectors) **X** and **Y** is (15)

coordinates. It is therefore important that the spatial resolution of the input image is high enough to enable the interpolation to the reference image resolution.

MEASUREMENT DATA

Newsprint paper samples that were printed with sheet-fed offset in a pilot press were examined. The printing layout contained various halftone and compact colour areas of which five were selected as test areas to be measured. The size of each test area was 22 by 15 mm. Exactly the same paper properties were measured from the test areas before and after printing. Firstly, optical formation/transmittance was measured with a scanner with illumination from the reverse side of the sheet. Secondly, the samples were scanned with reflective light so that images of paper brightness and print quality were obtained before and after printing, respectively. Thirdly, surface topography was

measured with a photometric stereo device that recovers the topography map from digital photographic images taken with different illumination directions (2). This device also provides photographic images of paper brightness and print quality, to be compared with the corresponding images acquired by scanner. The pixel size in all the measurements is approximately 10 μm in x and y directions.

Scanners and cameras were used to record the intensity values of red, green and blue light in separate channels. In case of unprinted white paper the colour channels contain almost equal planar variation. With printed samples the printing colour affects the variation captured by each channel. For instance cyan colour reflects blue and green light but blocks red wave lengths. Therefore the red channel best reveals the variation in print quality on cyan areas, whereas the blue and green channels mostly carry information about the paper, especially in transparent

$$f(\mathbf{x}, \mathbf{y})\mathbf{dxdy} = P(\mathbf{x} \le \mathbf{X} \le \mathbf{x} + \mathbf{dx}, \mathbf{y} \le \mathbf{Y} \le \mathbf{y} + \mathbf{dy}) \quad [1]$$

where P denotes probability. Correspondingly, the conditional pdf of random variable $\mathbf{y}$ given $\mathbf{x}$ is (15)

$$f(\mathbf{y}|\mathbf{x})\mathbf{dy} = P(\mathbf{y} \le \mathbf{Y} \le \mathbf{y} + \mathbf{dy}|\mathbf{x} = \mathbf{X}) \quad [2]$$

The regression of $\mathbf{Y}$ describes the expected value of this conditional density, thus it is a function of $\mathbf{x}$ (15):

$$E\{\mathbf{Y}|\mathbf{x}\} = \mu_y(\mathbf{x}) = \int_{-\infty}^{\infty} \mathbf{y}f(\mathbf{y}|\mathbf{x})\mathbf{dy} \quad [3]$$

If the joint probability density of $\mathbf{X}$ and $\mathbf{Y}$ is a multivariate Gaussian distribution, and if $\mathbf{X}$ and $\mathbf{Y}$ are correlated, the regression of $\mathbf{Y}$ is a linear function of $\mathbf{x}$. However, the joint probability densities of the property maps measured from paper are not Gaussian. This can be easily verified by the information-theoretic Kullback-Leibler distance, or relative entropy (19). This measures the distance between two probability distributions, $f_1(\mathbf{x})$ and $f_2(\mathbf{x})$:

$$D(f_1(\mathbf{x})\|f_2(\mathbf{x})) = \int_{-\infty}^{\infty} f_1(\mathbf{x})\log\left(\frac{f_1(\mathbf{x})}{f_2(\mathbf{x})}\right)d\mathbf{x} \quad [4]$$

The Kullback-Leibler (KL) distance, D, is always non-negative and zero only if and only if $f_1(\mathbf{x}) = f_2(\mathbf{x})$. If $f_2(\mathbf{x})$ is chosen as the Gaussian distribution estimate based on the data, then $f_2(\mathbf{x})$ is parameterized by one mean vector and one covariance matrix calculated from the data. Then choosing $f_1(\mathbf{x})$ as the histogram estimate or the GMM estimate of the pdf, permits the assessment of the appropriateness of Gaussian approximation to the pdf. The larger the KL distances, the more the distribution ($f_1(\mathbf{x})$) deviates from a Gaussian distribution. The Kullback-Leibler distances computed from the experimental data are reported in the following section.

Another statistical measure found useful in this work is the skewness of the conditional pdfs. The traditional measure of skewness is based on the third moment of the probability density. A skewness parameter based on the more robust order statistics has been used here for comparison. The values of percentiles, $b_{2.5}$, b_{50} and $b_{97.5}$, which are standard tabulated values in statistical literature (e.g. (15)), have been applied. In this case, percentiles were computed numerically from the estimated distributions as inverse values of the cumulative distribution function. The 50 % percentile, b_{50}, is the median value. The skewness parameter used in this work depends on the relation of the 2.5 %, 50 % and 97.5 % percentiles as follows:

$$skewness = \frac{b_{97.5} - b_{50}}{b_{50} - b_{2.5}} \quad [5]$$

According to this definition, the distribution is symmetric when skewness equals one. As shown in the following section, the probability distributions computed from the property maps measured from paper are typically strongly skewed.

As the joint distributions are not Gaussian, there are more appropriate methods to analyze the dependencies than linear regression. Principal component analysis (PCA) (20) and independent component analysis (ICA) (21) can give an insight into the sources of variation in the data by revealing statistically significant dimensions in the multivariate data space. However, the most complete description of the statistical dependencies between the measured variables is provided by the joint probability density functions.

There are two ways to proceed with the non-Gaussian joint pdfs: by describing the interrelationship of the variables by their joint histogram, or by choosing a parametric model for the joint pdf and identifying the model parameters. In the latter case, the Gaussian mixture model (GMM) (16) is a very attractive choice due to its simple and efficient formulation. GMM approximates the probability density function of a d-dimensional random variable $\mathbf{X}$ as a weighted sum of N Gaussian distributions:

$$f(\mathbf{x}) =$$
$$\sum_{i=1}^{N} c_i (2\pi)^{-d/2} (\det(\mathbf{C}_i))^{-1/2} \exp\left[-\frac{1}{2}(\mathbf{x} - \mu_i)^T \mathbf{C}_i^{-1}(\mathbf{x} - \mu_i)\right] \quad [6]$$

Each Gaussian component is parameterized by its mean, μ_i, and covariance matrix, $\mathbf{C}_i$. The weights, c_i, of the Gaussians components are called the priors. With sufficiently high number of component distributions, GMM is capable of describing practically any continuous distribution (22). The parameters of GMM model are typically estimated by the expectation maximization (EM) algorithm (23).

The joint pdf estimation – either through histogram, GMM or any other method – provides several possibilities for further analysis. Firstly, nonlinear regression can be computed from the joint density by applying Equation 3. Secondly, the different levels of probability in the joint pdf can be examined to form anomaly maps. They reveal the points and areas of the multivariate image that most extremely deviate from the typical statistical behavior of the data. The condition for an observation vector $\mathbf{x}$ at location i to be abnormal to degree p is given as

$$f(\mathbf{x}) < C(p) \quad [7]$$

where $f(\mathbf{x})$ is the probability density function of $\mathbf{x}$ and the relationship between C and p is determined through

$$p = p(C) = \int_{f(\mathbf{x})<C} f(\mathbf{x})dx \quad [8]$$

In practice, the abnormality degree, p (e.g. 2.5 %), is first chosen. A suitable upper limit, C, is then determined for the probability density so that the integral in Equation 8 equals p. The anomaly map is obtained by making a mask where locations i that satisfy the condition 7 are given a value one whereas all other locations of the mask assume value zero.

Thirdly, the tails of the conditional probability densities can be examined to detect exceptional values on the (print quality) maps. As anomaly maps are based on joint pdfs and tail analysis on conditional pdfs, not all of these latter exceptional values are in the anomaly maps. Finally, the tail areas and the points indicated by the anomaly maps can be overlaid with the original 2D measurement maps. Now it is easy to visualize the points and local areas that show exceptional behavior. The possible concentration of the anomalies on the measured maps indicates disturbances in the process that produced the data.

RESULTS OF MULTIVARIATE STATISTICAL ANALYSIS

The objective of this work is to find and describe the probabilistic dependencies between print quality and the physical structure of unprinted paper. The results presented here concentrate on the joint probability distributions of surface topography and print quality on two different types of test areas. The print quality is described by the photographic image of the test area, taken after printing. The common size of the analyzed 2D maps on each test area (after discarding the geometrically distorted parts) is typically around 20 by 13 mm but a smaller area has been chosen here to show more details. The illustrations present a 5 by 5 mm
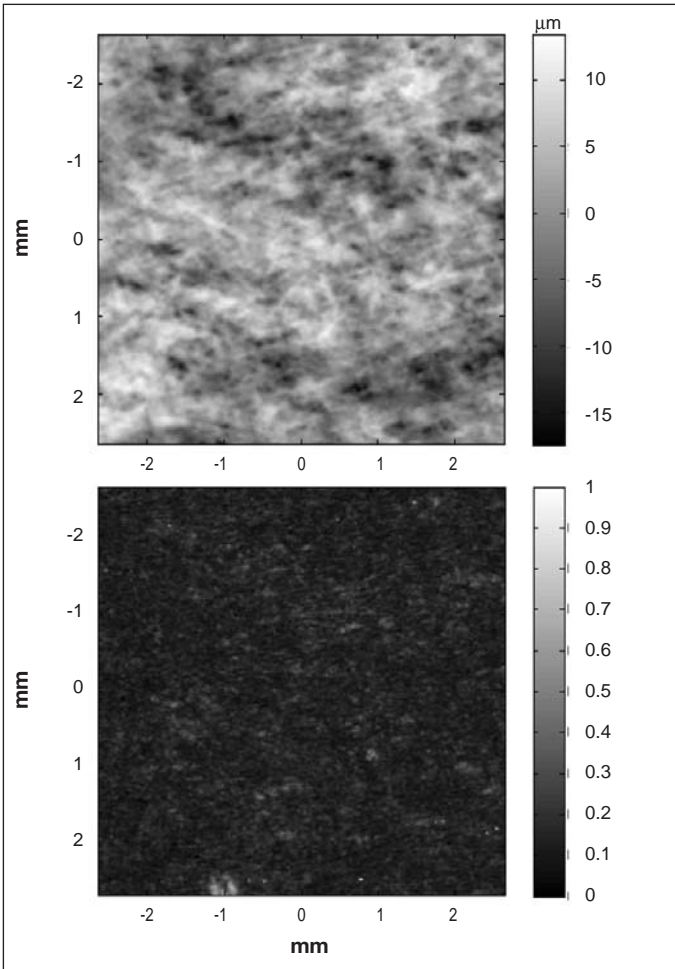
Fig. 3　Surface topography (top) and aligned photographic reflectance image of print quality (bottom) on a 5 by 5 mm area.
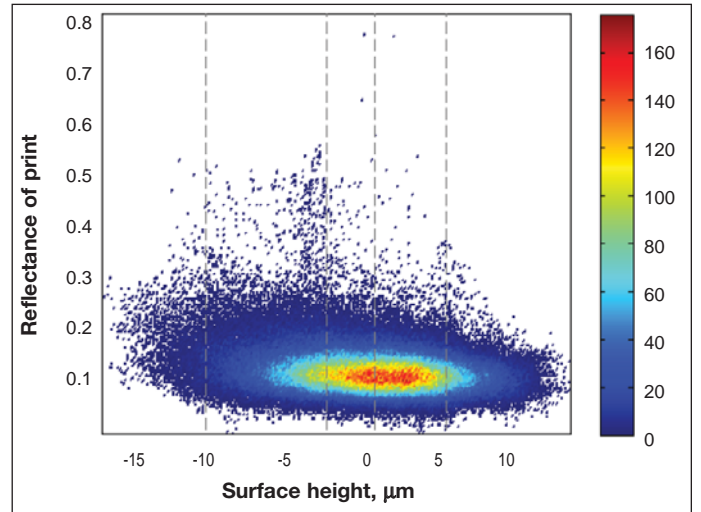

Fig 4　Joint histogram of surface topography and print quality measurements. The vertical dashed lines indicate the sampling points of the conditional pdfs shown in Figure 5.

selection of a test area that was printed with compact cyan so that only the cyan printing roll pressed the test area. There was neither water application nor back-trap conditions present on this test area. The other type of test area examined in this work was printed with compact cyan in normal 4-colour offset conditions with water and back-trap. Eight newsprint paper sheets were examined, each sheet containing one test area of each type of cyan printing.

In the analysis, both joint histograms and GMM-based pdfs are used to describe the data. By comparing the GMM-based distribution models with histograms it is possible to ensure that all the essential details of the data have been taken into account in GMM. As GMM can describe very complicated distributions with a moderate number of parameters, it is the main tool used in the analysis. Furthermore, GMM enables the analytical calculation of conditional probability densities and statistical parameters such as cumulants and moments.

An example is given of the analysis of

two 2D maps, surface topography and photographic reflectance image of print quality, measured from exactly the same area. The aligned maps are shown in Figure 3. There are light spots in the reflectance (print quality) map due to low local density or missing printing ink. These spots cause the scattering on the upper edge of the joint histogram shown in Figure 4. The three-dimensional histogram is shown from above and the heights of the bins are presented by the different colours. In Figure 4 it is notable that the joint pdf is skewed towards the higher values of reflectance. A closer look at the skewness and the shape of the tails of the conditional distributions is presented in Figure 5. It shows selected vertical 'slices' of the joint pdf estimated by both the histogram (slightly smoothed with a sliding Gaussian kernel) and a 10-component GMM. In Figure 5 the conditional pdfs are presented on logarithmic scale to emphasize the tails of the conditional distributions.

The regression of print quality according to Equation 3, using the maps in Figure 3, is non-linear due to the non-

Gaussian shape of the joint pdf. The regression curves as conditional expected values and their uncertainties are presented in Figure 6 for both the GMM and histogram approach. Notable increase in the reflectance value is expected as the pits in the paper surface get deeper. Instead of a least-squares linear fit over the total data set, the nonlinear regression is computed at each value of surface height from the conditional pdf of reflectance. GMM provides a particularly easy access to the regression estimate that can be calculated analytically from the model parameters. Furthermore, the unstable behavior of regression estimate at the edges of the data value range, resulting from the relatively low number of observations, is avoided in the GMM approach. However, it should be noted that 99 % of the surface height values in this case lie between -11 µm and +10 µm. As there are hardly any data points beyond this range, the regression estimates as well as the Kullback-Leibler distances and skewness values presented in the following are unreliable at the extreme values of surface height.

Figure 7 presents the Kullback-Leibler (KL) distances between the GMM-based conditional pdfs of print quality and the corresponding single Gaussian models. Throughout the surface height range, the KL distance is higher than zero, which was expected from the non-Gaussian shape of the conditional pdfs. It can also be seen that the KL distance decreases as the surface height values increase until the height value reaches 10 µm. Beyond this height the results are unreliable due to the low number of observations. The decrease in KL distance corresponds to
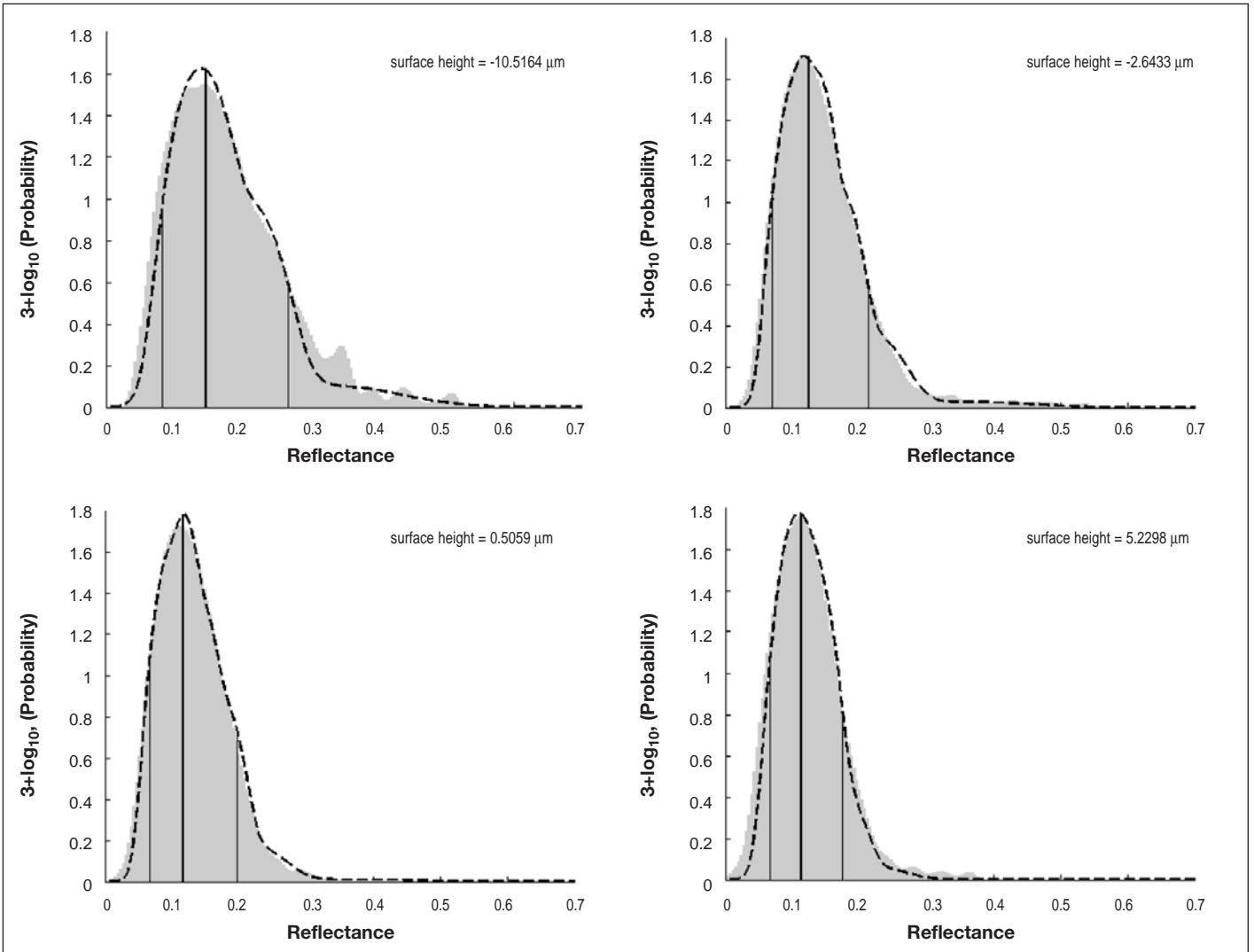
Fig. 5 Histogram-based (gray bars) and GMM-based (dashed black line) conditional pdfs of print quality at the values of surface height shown in Figure 4. The vertical lines indicate 2.5 %, 50 % and 97.5 % percentiles computed from GMM.
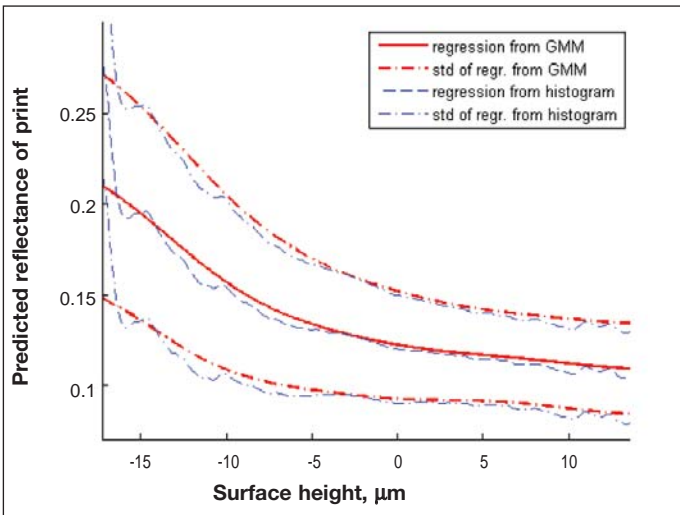

Fig. 6 Regression curves plus/minus their standard deviations computed from GMM (red) and from histogram (blue).
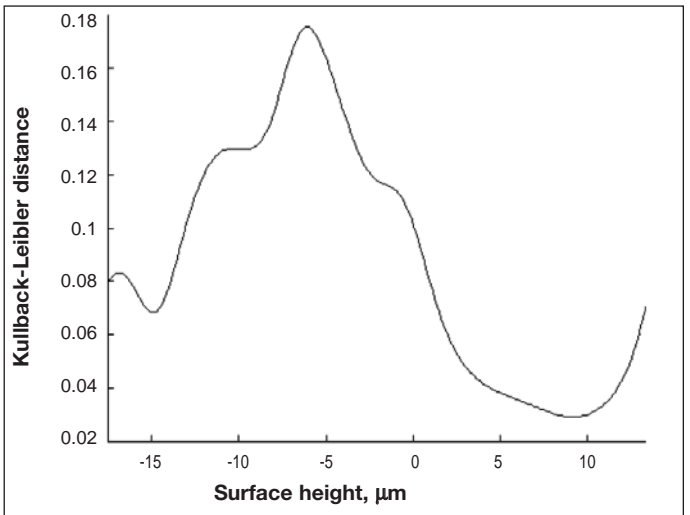

Fig. 7 Kullback-Leibler distance of conditional pdfs of print quality, computed through GMM.

the narrowing of the joint histogram in Figure 4 towards a more Gaussian shape. A similar shape to that of the KL curve can be seen in Figure 8 that presents the skewness of the conditional pdfs of print quality computed according to Equation 5. The visual analysis of all the 16 cyan test areas (eight with normal printing conditions and eight without back-trap) has suggested that the skewness parameters and KL distances are related to the amount of print defects. Based on visual inspection, the areas printed without back-trap typically contain clearly visible print defects whereas the normal cyan
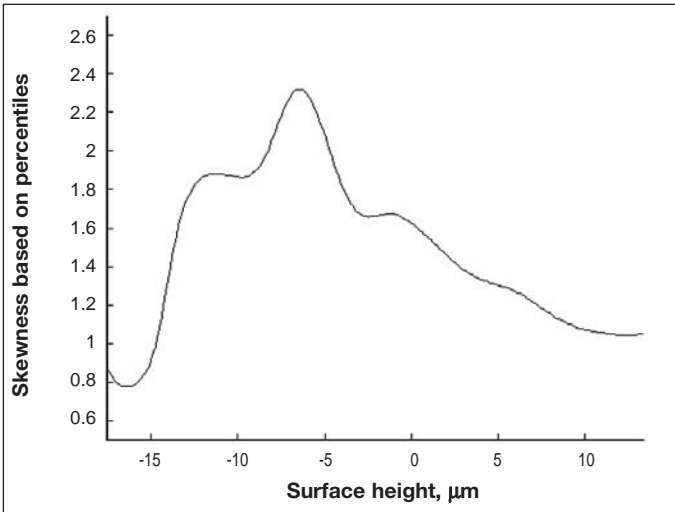
Fig. 8 Skewness of conditional pdfs of print quality, based on the percentiles computed from GMM.
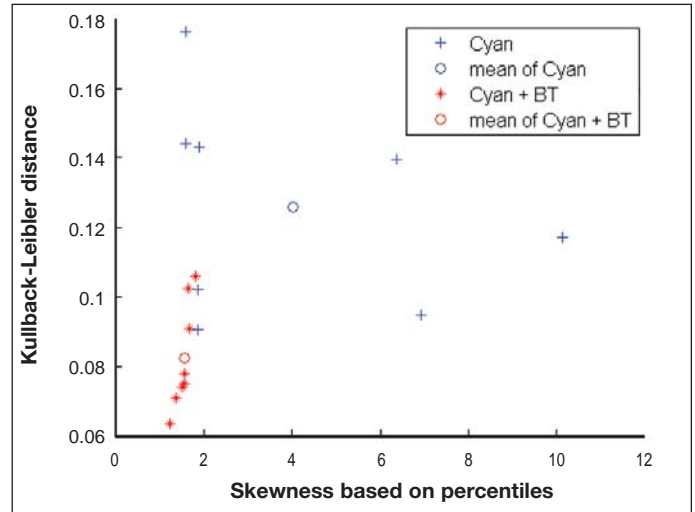

Fig. 9 Skewness parameters and KL distances of the 16 test areas. The blue marks denote the non-back-trap cyan samples and red marks denote the normal cyan areas.
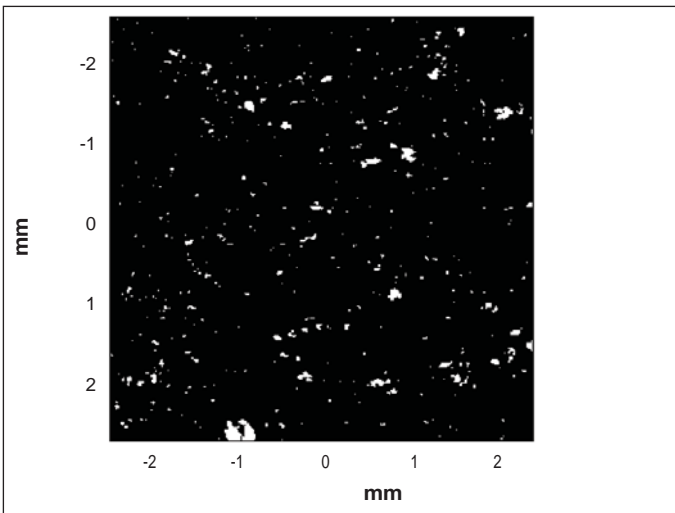

Fig. 10 Joint pdf based anomaly map indicating (by white) the points in Figure 3 that occur with less than 2.5 % probability.
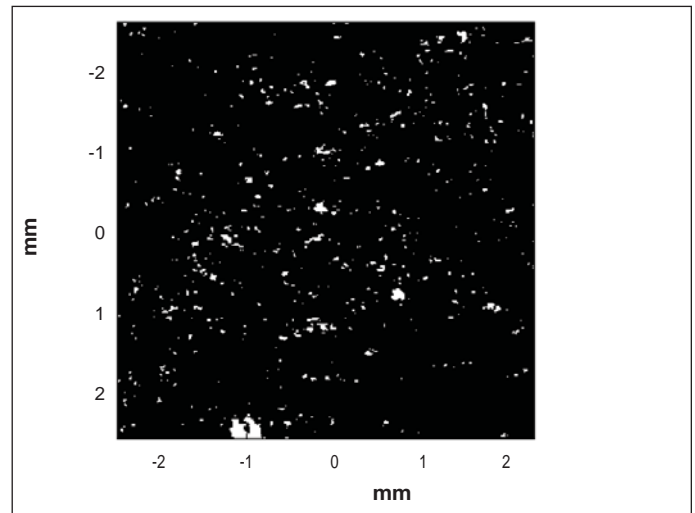

Fig. 11 Mask indicating (by white) the points in the print quality map that are exceptionally bright based on the 2.5 % percentile tails of the conditional pdfs of print quality.

areas have only very small and few light spots, if any. The print defects skew the joint histogram towards the high values of reflectance and thus increase the skewness measure and Kullback-Leibler distance. To summarize the behavior of these parameters in the different printing settings, the shape of the conditional pdf of print quality, subject to the condition that the surface height value is below zero, was examined. This limits the inspection to the areas where valleys or pits in the surface may have caused print defects. The skewness parameter and KL distance have been computed from the conditional pdf of print quality of each of the 16 test areas. The results are illustrated in Figure 9. When the eight non-back-trap cyan areas are compared to the eight normal cyan areas, the average KL distance increases

approximately 50 % and the average skewness more than doubles.

Anomaly maps can be derived from the joint pdf by thresholding according to a chosen level of probability. Figure 10 presents an anomaly map that reveals those points from the surface topography and print quality maps of Figure 3 that occur with less than 2.5 % probability according to their joint probability distribution. As the likelihood of these observations is very small, they cannot be expected to be explained by the regression model. For comparison, Figure 11 shows a mask that detects exceptional points in the print quality map based on the low probability tail areas of the conditional pdfs. While the mask in Figure 11 efficiently detects the points where the reflectance measured from the print is

exceptionally high, the mask in Figure 10 introduces the effect of the combined exceptionality of surface height value and print quality. The comparison of these masks provides information about the role of surface topography in the occurrence of print defects.

DISCUSSION

This study has been limited to printing newsprint paper with sheet-fed offset even though this is not commercially relevant. Newsprint was chosen for the experiments because a relatively clear view of the effect of surface topography on print quality was wanted, without the additional complexity caused by coating. Sheet-fed offset was chosen because it was the only production-scale printing

method that enabled controlled measurements before and after printing.

The unusual printing conditions may partly explain the large variance of the skewness and Kullback-Leibler results seen in Figure 9. This is particularly likely for the non-back-trap test areas where neither water application nor back-trap conditions were present. Various factors other than surface topography, for instance surface strength, have obviously affected the print quality in this experiment. It will be possible to further verify the feasibility of the probabilistic analysis framework as new printing data sets become available from, e.g., gravure printing experiments.

CONCLUSIONS

A two-phase image registration procedure for robust and accurate automatic registration and alignment of randomly textured images has been developed and implemented. Successful sub-pixel alignment of the 2D measurements has enabled the probabilistic joint analysis of print quality and surface topography maps measured from exactly the same area. The large amount of multivariate pointwise data in the aligned property maps provides a strong basis for statistical inference.

The objective of the work is to find and describe the dependencies between print quality and the physical structure of unprinted paper. These dependencies are probabilistic rather than deterministic, and therefore the joint probability distributions of the measured variables are needed to reveal the essential information. The joint pdfs have been described by histograms and Gaussian mixture models. The skewness and Kullback-Leibler distance parameters have been computed from the pdfs,

and the usefulness of these parameters in the characterization of the probability densities and, finally, print quality has been illustrated. Anomaly maps have also been formed from the joint pdfs to reveal the low probability, high importance, print defects and to evaluate their origins.

As indicated in this work, multivariate analysis in terms of joint pdfs is an important link between the combined effect of unprinted paper properties, processing conditions and the quality of print – directly measurable as a map of colour variation. It is expected that these methods will find wide application in analyzing the structural dependencies of paper and board quality.

REFERENCES

(1) Norman, B. and Wahren, D. – Mass distribution and sheet properties of paper, *Trans. 5th Fund. Res. Symp.*, (ed. F. Bolam), Cambridge, p. 7 (1973).

(2) Hansson, P. and Johansson, P-Å. – Topography and reflectance analysis of paper surfaces using a photometric stereo method, *Optical Engineering* **39**(9):2555 (2000).

(3) Chinga, G., Johnsen, P.O., Dougherty, R., Lunden-Berli, E. and Walters, J. – Quantification of the 3D microstructure of SC surfaces, *J. Microscopy* **227**(3):254 (2007).

(4) Sung, Y. J., Ham, C. H., Kwon, O., Lee, H. L. and Keller, D. S. – "Application of thickness and apparent density mapping by laser profilometry," *Trans. 13th Fund. Res. Symp.,* (ed. S.J. I'Anson), Cambridge, p. 961 (2005).

(5) Fetsko, J. M. and Zettlemoyer, A. C. – Factors affecting print gloss and uniformity, *Tappi* **45**(8):667 (1962).

(6) Lyne, B. – Machine-calendering: implications for surface structure and printing properties, Tappi **59**(8):101 (1976).

(7) Oittinen, P. and Saarelma, H. – **Printing**, Fapet, Finland, p. 214 (1998).

(8) Kajanto, I. M. – Pointwise dependence between local grammage and local print density, *Paper and Timber* **73**(4):338 (1991).

(9) Mangin, P. J., Béland, M.-C. and Cormier, L. M. – A structural approach to paper surface compressibility – Relationship with printing

characteristics, *Trans. 10th Fund. Res. Symp.,* (ed. C.F. Baker), Oxford, p. 1397 (1993).

(10) MacGregor, M. A., Johansson, P.-Å. and Béland, M.-C. – Measurement of small-scale gloss variation in printed paper, *Proc. 1994 Int. Printing and Graphics Arts Conf.,* Halifax, p. 33 (1994).

(11) Brown, L. – A Survey of image registration techniques, *ACM Computing Surveys* **24**(4):325 (1992).

(12) Althof, R.J., Wind, M.G.J. and Dobbins, J.T. – A rapid and automatic image registration algorithm with subpixel accuracy, *IEEE Trans. Medical Imaging* **16**(3):308 (1997).

(13) Liu, J., Vemuri, B. C. and Marroquin, J. L. – Local frequency representations for robust multimodal image registration, *IEEE Trans. Medical Imaging* **21**(5):462 (2002).

(14) Lähdekorpi, M., Ihalainen, H. and Ritala, R. – Using image registration and alignment to compare alternative 2D measurements, *Proc. XVIII IMEKO World Congress*, Rio de Janeiro (2006).

(15) Papoulis, A. – **Probability & Statistics**, Prentice-Hall, USA, p. 98-239 (1990).

(16) Nabney, I. T. – **Netlab: Algorithms for pattern recognition,** Springer-Verlag, UK, p. 79-113 (2002).

(17) Heiskanen, I. – **Two-dimensional small-scale mapping methods in predicting flexographic printability of board**, Licentiate thesis: Lappeenranta University of Technology, Finland (2005).

(18) Wolberg, G. – **Digital image warping**, IEEE Computer Society Press, USA, p. 47 (1990).

(19) Cover, T. and Thomas, J. – **Elements of information theory**, John Wiley & Sons, USA, p. 18 (1991).

(20) Geladi, P. and Grahn, H. – **Multivariate image analysis**, John Wiley & Sons, UK, p. 87 (1996).

(21) Hyvärinen, A., Karhunen, J. and Oja, E. – **Independent component analysis**, John Wiley & Sons, USA (2001).

(22) Bishop, C. M. – **Pattern recognition and machine learning**, Springer-Verlag, USA, p. 110 (2006).

(23) Figueiredo, M. A. T. and Jain, A. K. – Unsupervised learning of finite mixture models, *IEEE Trans. Pattern Analysis and Machine Intelligence* **24**(3):381 (2002).